

# Bifurcation sequences in the interaction of resonances in a model deriving from nonlinear rotordynamics: the zipper

G.H.M. van der Heijden\*

November 1, 1999

## Abstract

Using numerical continuation we show a new bifurcation scenario involving resonant periodic orbits in a parametrised four-dimensional autonomous system deriving from nonlinear rotordynamics. The scenario consists of a carefully orchestrated sequence of transcritical bifurcations in which branches of periodic solutions are exchanged. Collectively, the bifurcations resemble the action of a zipper. An underlying governing mechanism clearly exists but still has to be uncovered.

For a range of parameter values the sequence of bifurcations forms a global connection between a Šil'nikov bifurcation and (partial) mode-locking. The homoclinic bifurcation is introduced into the system by a Takens-Bogdanov bifurcation. The system also features an interaction between two chaotic Šil'nikov bifurcations.

## 1 Introduction

Mode-locking is a common phenomenon in nonlinear dynamics occurring, for instance, in forced systems of coupled oscillators. In the simplest case of a single driven oscillator one then observes resonance tongues in parameter space, inside which a pair of periodic orbits exist with a frequency which is a rational multiple of the driving frequency. The boundaries of the resonance regions are curves of saddle-node bifurcations of these periodic orbits. For sufficiently small forcing the periodic orbits lie on invariant tori, and the situation is adequately described by circle maps [3, 23].

More generally, in the case of more than one oscillator we can have multiply-periodic (toroidal) motion. Different levels of mode-locking are then possible depending on the number of rational relations between the frequencies involved. Fully mode-locked periodic motion is obtained if between  $k$  frequencies  $k - 1$  independent relations are present. If fewer relations exist one speaks of partial mode-locking. This multiple-frequency resonance requires a description in terms of torus maps [4], and much more complicated behaviour is possible than in the simple case of a single oscillator.

As another example, in autonomous systems mode-locking is often associated with a secondary Hopf bifurcation at which an invariant torus bifurcates from a periodic orbit [2]. Motion on the torus will in general be mode-locked.

---

\*Centre for Nonlinear Dynamics, University College London, Gower Street, London WC1E 6BT, UK.

Unless the system has a special symmetry, in all these cases one generally has infinitely many resonance tongues. For a suitable small parameter (in driven systems, typically, forcing amplitude) the tongues are disjoint, but as the parameter is increased they may start to overlap. For the corresponding parameters we then have coexisting periodic solutions. It is well-known that very complicated bifurcation sequences may occur in the regions of overlap [3].

Another well-known mechanism for the creation of (infinite) families of periodic solutions is provided by homoclinic orbits. For instance, near a homoclinic orbit to a saddle-focus-type fixed point, often called a Šil'nikov-type homoclinic orbit, we have, under some conditions on the eigenvalues of the fixed point, the existence of horseshoes [24]. In particular, this implies the existence of a countable infinity of periodic orbits with arbitrarily high period.

Both mechanisms, mode-locking and homoclinic bifurcation, can successfully be studied analytically locally (for instance, near a secondary Hopf or Šil'nikov bifurcation, respectively). The periodic orbits, however, are often very robust and keep existing for parameters well away from the regions where these analytical studies are valid, indeed where the source of the multitude of periodic orbits (an invariant torus or a homoclinic orbit) may long have ceased to exist. It is therefore conceivable that families of periodic solutions of both mechanism are globally connected, i.e., that by varying parameters, periodic orbits involved in mode-locking can gradually evolve into periodic orbits associated with a homoclinic bifurcation (of Šil'nikov type, say).

Connections between resonances and homoclinic orbits have been known for quite some time. For instance, they occur in time-periodically perturbed planar oscillators which, in the unperturbed system, have a one-parameter family of periodic orbits inside a homoclinic connection. To such systems a subharmonic and homoclinic Melnikov analysis [24] can be applied, showing the accumulation of resonance tongues onto lines of homoclinic tangencies bounding a homoclinic wedge. For an early reference see [15]. This behaviour is consistent with the work of Gavrilov and Šil'nikov (see [16, 24] for summaries, and [19] for more recent work in this direction). An accumulation of resonance tongues onto lines of homoclinic or heteroclinic tangencies should also be expected when a line of secondary Hopf bifurcations and an appropriate line of homoclinic or heteroclinic bifurcations meet. For instance, Kirk [21, 22] studied a parametrised family of three-dimensional vector fields containing the truncated normal form of the saddle-node/Hopf bifurcation (one zero eigenvalue and two imaginary ones). Resonance tongues were found to emerge from a curve of secondary Hopf bifurcations and to accumulate on heteroclinic tangencies. Other cases have been reported in [18, 19].

In this paper we study a strongly nonlinear four-dimensional system with a different, more global, connection between resonances and homoclinic bifurcations. Our system will not have a secondary Hopf bifurcation. Rather, the organising centre of the dynamics will turn out to be a Takens-Bogdanov bifurcation. The system we consider is:

$$\begin{aligned}
 \dot{x}_1 &= x_2 + \omega x_3 \\
 \dot{x}_2 &= \omega x_4 - \gamma x_2 - \left(1 - \frac{\delta}{\sqrt{x_1^2 + x_3^2}}\right) x_1 + \epsilon \omega^2 \\
 \dot{x}_3 &= -\omega x_1 + x_4 \\
 \dot{x}_4 &= -\omega x_2 - \gamma x_4 - \left(1 - \frac{\delta}{\sqrt{x_1^2 + x_3^2}}\right) x_3.
 \end{aligned} \tag{1}$$

In [17] this system was arrived at by (trivially) reducing a driven system of two coupled oscillators that was studied as a model for nonlinear rotordynamics. Specifically, the original rotor

system was given by

$$\ddot{y} + \gamma \dot{y} + \left(1 - \frac{\delta}{|y|}\right) y = \epsilon \omega^2 e^{i\omega t}, \quad (2)$$

where  $y = y_1 + iy_2$  is a complex co-ordinate measuring the rotor's deflection from its rest position. The parameter  $\omega$  is the driving frequency,  $\epsilon$  is the mass eccentricity of the rotor,  $\gamma$  is a linear damping coefficient, and  $\delta$  is the bearing clearance, the only source of nonlinearity in the system. Note that (2) has rotational symmetry. Indeed, (1) is obtained from (2) by passing to a co-rotating co-ordinate system  $z = ye^{-i\omega t}$ , changing to a first-order system and additionally performing a simple linear transformation. We refer to [17] and references therein for the relevance of (2) and similar models in nonlinear rotordynamics.

In fact, (2) is not a complete model of the lateral deflections of a rotor with bearing clearance, as is evidenced by the singularity for zero radial deflection  $r := \sqrt{y_1^2 + y_2^2} = \sqrt{x_1^2 + x_2^2}$ . Normally, one would specify a different set of equations for motion inside the bearings, i.e., when  $r < \delta$ . In this paper, however, this will not concern us and we will treat (1) mainly as an abstract dynamical system providing an interesting case study in nonlinear dynamics (although we do have something to say about experiments on rotor systems in Section 5). It will turn out that in practice, e.g., in numerical experiments on (1), the singularity at the origin poses no problems.

We should emphasise that the system could be simplified further by scaling out the parameter  $\epsilon$ . We leave it in mainly for 'historical' reasons. The parameter is however not used as an independent parameter but fixed to 0.1 throughout the main part of this paper, so numerical results of a further scaled system can simply be found by appropriate multiplication by a constant. The damping coefficient  $\gamma$  will also not be used as a bifurcation parameter, although we will contrast the cases of strong and moderate damping. System (1) is thus treated as a two-parameter family of four-dimensional vector fields. Homoclinic orbits will be introduced into the system by a Takens-Bogdanov bifurcation.

Locally, the Takens-Bogdanov bifurcation can be studied in a two-dimensional centre manifold. More complicated, non-planar, dynamics, however, is found as we move away from this codimension-two singularity, and the homoclinic bifurcation becomes of Šil'nikov type. In these regions of parameter space we have to resort to numerical techniques in order to trace out different types of solutions. We use the continuation and bifurcation package AUTO [9, 10] in conjunction with direct integration of the differential equations to follow the periodic solutions away from the Šil'nikov bifurcation.

It turns out that through a masterly orchestrated sequence of bifurcations, resembling the action of a zipper, these periodic solutions ( $n$ -loops) become involved in mode-locking phenomena. This mode-locking aspect of the  $n$ -loops was studied in detail in [17] by taking  $\delta$  to be a small parameter (see Section 4 for a brief summary). There, it proved useful to adopt the viewpoint of the unreduced driven system (2) with phase space  $\mathbb{R} \times S^1$ . The periodic solutions then correspond to partially mode-locked 2-tori in three-frequency resonance. In this paper we establish the connection with homoclinic orbits by treating (1) as a strongly nonlinear system, i.e., by taking  $\delta$  'large'.

The outline of the rest of this paper is as follows. In Section 2 we analyse bifurcations of fixed points of (1). In Section 3 we numerically investigate the global dynamics concentrating on the many periodic solutions of the system. First the relatively simple case of strong damping is treated. Then the considerably more complicated case of moderate damping is considered. Here

we encounter the zipper mediating between homoclinic orbits and mode-locking. Mode-locking is not central to the present discussion, but, for completeness, in Section 4 the relevant results from [17] are briefly reviewed. In Section 5, finally, we point to some related results in the literature, discuss some experimental work reported and make some concluding remarks.

## 2 Bifurcations of fixed points

Fixed points of (1) are given by

$$x_1 = \frac{(1 - \omega^2)r^2 - \delta r}{\epsilon\omega^2}, \quad x_2 = -\omega x_3, \quad x_3 = \frac{-\gamma r^2}{\epsilon\omega}, \quad x_4 = \omega x_1, \quad (3)$$

where  $r$  solves

$$[\gamma^2\omega^2 + (\omega^2 - 1)^2]r^2 + 2(\omega^2 - 1)\delta r + \delta^2 - \epsilon^2\omega^4 = 0. \quad (4)$$

Typical frequency-response curves are given in Fig. 1. There are two cases which are separated by a codimension-two bifurcation at  $\delta = \delta_{\text{TC}}$  which we will shortly discuss in more detail.

The characteristic polynomial of the Jacobian matrix at a fixed point is

$$P(\lambda) = \lambda^4 + a_3\lambda^3 + a_2\lambda^2 + a_1\lambda + a_0, \quad (5)$$

where

$$a_0 = \frac{\delta}{r}(\omega^2 - 1) + \gamma^2\omega^2 + (\omega^2 - 1)^2, \\ a_1 = -\gamma \left( \frac{\delta}{r} - 2(\omega^2 + 1) \right),$$

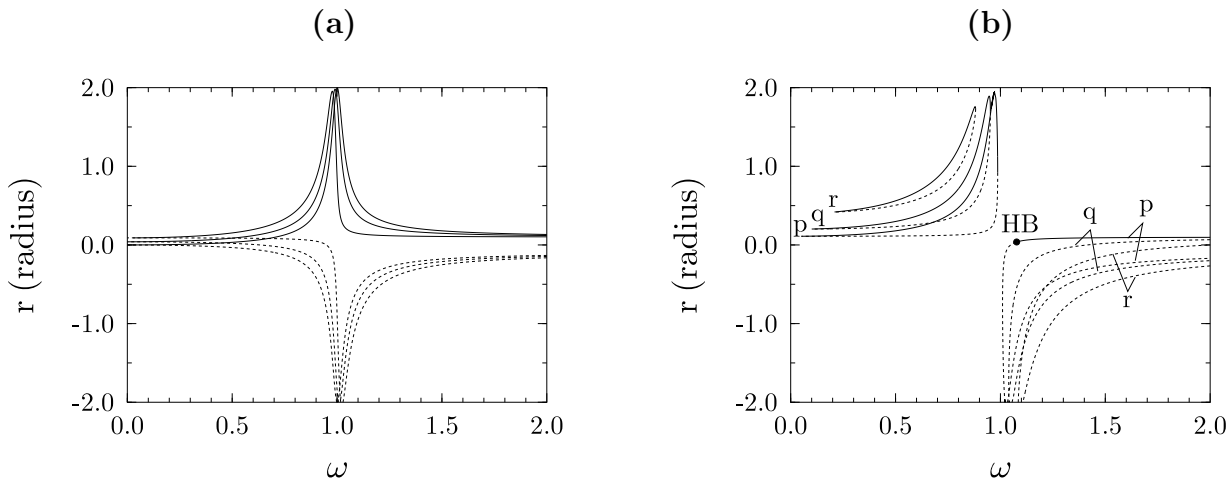


Figure 1: Curves of fixed points in the dissipative case. Solid lines represent stable equilibria, dashed lines unstable or non-physical ones. (a)  $\delta < \delta_{\text{TC}}$ :  $\delta = 0.0, 0.04, 0.09$ , (b)  $\delta > \delta_{\text{TC}}$ :  $\delta = 0.11$  (p),  $0.2$  (q),  $0.4$  (r). HB denotes a Hopf bifurcation. ( $\epsilon = 0.1$ ,  $\gamma = 0.05$ .)

$$a_2 = -\frac{\delta}{r} + 2(\omega^2 + 1) + \gamma^2,$$

$$a_3 = 2\gamma.$$

Several local bifurcations of codimension one and two are possible which we will now discuss.

## 2.1 Codimension-one bifurcations

Saddle-node bifurcation: For a simple zero eigenvalue (all other eigenvalues having non-zero real parts) we need:

$$a_0 = 0, \quad a_1 \neq 0. \quad (6)$$

Hopf bifurcation: Substituting  $\lambda = i\nu$ ,  $\nu \in \mathbb{R}$ ,  $\nu \neq 0$ , into (5) we derive the conditions

$$\frac{a_1}{a_3} \left( \frac{a_1}{a_3} - a_2 \right) + a_0 = 0, \quad \nu^2 = \frac{a_1}{a_3}. \quad (7)$$

Because  $a_3 > 0$  it follows that  $a_1 > 0$ , or

$$\frac{\delta}{r} < 2(\omega^2 + 1). \quad (8)$$

The four eigenvalues are given by

$$\lambda_{1,2} = \pm i\Omega, \quad \lambda_{3,4} = -\gamma \pm i\Omega, \quad \text{whith} \quad \Omega = \sqrt{\omega^2 + 1 - \frac{\delta}{2r}},$$

where  $r$  is a solution of (4) and the other parameters are such that the first equation in (7) is satisfied.

We shall treat  $\epsilon$  and  $\gamma$  as constants and study bifurcation curves in the  $\omega$ - $\delta$  plane. Close to a Hopf bifurcation the eigenvalues are  $\alpha_1(\mu) \pm i\omega_1(\mu)$ ,  $\alpha_2(\mu) \pm i\omega_2(\mu)$ , with  $\alpha_1(\mu_c) = 0$ ,  $\alpha_2(\mu_c) = -\gamma$  and  $\omega_1(\mu_c) = \omega_2(\mu_c) = \Omega$ , where  $\mu$  is a bifurcation parameter (either  $\omega$  or  $\delta$ ). If the transversality condition

$$\alpha'_1(\mu_c) \neq 0 \quad (9)$$

is satisfied then the Hopf bifurcation is characterised by the normal form at the critical value  $\mu_c$ . After a centre-manifold reduction this normal form (in polar co-ordinates) is given by (cf. [16])

$$\begin{aligned} \dot{r} &= cr^3, \\ \dot{\theta} &= \Omega + dr^2, \end{aligned} \quad (10)$$

provided  $c$  is non-zero. The coefficient  $c$  determines the stability of the emerging periodic orbit. Although in principle it is clear how to obtain  $\alpha'_1(\mu_c)$  and the normal form coefficients in (10), the computations become rather tedious, involving finding roots of the fourth-degree polynomial  $P(\lambda)$  in (5), so in checking the transversality condition (9) we shall content ourselves with a numerical computation, using Maple's arbitrary-precision arithmetic.

Note that if  $a_1/a_3 = a_2$  then  $\delta/r = 2(\omega^2 + 1) + 2\gamma^2$ , violating (8). In that case we would not have a Hopf bifurcation. In view of (7) this means that we cannot have a combined saddle-node/Hopf bifurcation. In particular, the conditions in (6) are necessary and sufficient for a

nondegenerate saddle-node bifurcation. The only degeneracy occurs if  $a_0 = a_1 = 0$ , in which case  $\delta/r = 2(\omega^2 + 1)$  and hence  $a_2 = \gamma^2 \neq 0$ . This case corresponds to a nondegenerate Takens-Bogdanov bifurcation as will be demonstrated below.

It can be verified that in the limit  $\omega \rightarrow \infty$  we have  $\delta_{\text{Hopf}} = 2\epsilon$ , independent of  $\gamma$ , and the eigenvalues become  $\lambda_{1,2} = \pm i\omega$ ,  $\lambda_{3,4} = -\gamma \pm i\omega$ . So, there is no Hopf bifurcation for  $\delta \geq 2\epsilon$ . Note that this is consistent with the data for  $\epsilon = 0.1$  presented in Fig. 1 showing only a (supercritical) Hopf bifurcation for  $\delta = 0.11$ .

## 2.2 Codimension-two bifurcations

Takens-Bogdanov bifurcation: If both  $a_0$  and  $a_1$  are zero in (5) then the eigenvalues are 0, 0,  $-\gamma$ ,  $-\gamma$  and the Jordan normal form of the Jacobian matrix is given by

$$\begin{pmatrix} 0 & 1 & 0 & 0 \\ 0 & 0 & 0 & 0 \\ 0 & 0 & -\gamma & 1 \\ 0 & 0 & 0 & -\gamma \end{pmatrix}. \quad (11)$$

This means that at the codimension-two bifurcation the fixed point has an attracting two-dimensional centre manifold which, in normal co-ordinates, is tangential to the generalised eigenspace of the matrix

$$\begin{pmatrix} 0 & 1 \\ 0 & 0 \end{pmatrix}.$$

Some algebra yields that the codimension-two singularity has the critical parameter values

$$\omega_{\text{TB}}^2 = \frac{1}{6} \left( 2 - \gamma^2 + \sqrt{16 - 4\gamma^2 + \gamma^4} \right), \quad \delta_{\text{TB}}^2 = \frac{2\epsilon^2 \omega_{\text{TB}}^4 (\omega_{\text{TB}}^2 + 1)^2}{3\omega_{\text{TB}}^4 + 4\omega_{\text{TB}}^2 + 1}, \quad (12)$$

while for the radius we have

$$r_{\text{TB}} = \frac{\delta_{\text{TB}}}{2(1 + \omega_{\text{TB}}^2)}. \quad (13)$$

A tedious normal form calculation of the centre-manifold-reduced vector field gives to second order the Bogdanov normal form [16]

$$\begin{aligned} \dot{x} &= y, \\ \dot{y} &= ax^2 + bxy, \end{aligned}$$

with coefficients

$$\begin{aligned} a &= -2 \frac{9z^6 + 6z^5 - 17z^4 - 12z^3 + 7z^2 + 6z + 1}{\epsilon \gamma^5 z^2}, \\ b &= -4 \frac{9z^7 + 15z^6 - 11z^5 - 29z^4 - 5z^3 + 13z^2 + 7z + 1}{\epsilon \gamma^6 z^3}, \end{aligned} \quad (14)$$

where

$$z = \omega_{\text{TB}}^2.$$

Thus we identify the codimension-two bifurcation as a Takens-Bogdanov bifurcation.

An interesting feature of the above normal form is that in the conservative limit the coefficients  $a$  and  $b$  both diverge, viz.,

$$a = \frac{1}{\epsilon} \left( -\frac{8}{\gamma} + 2\gamma - \frac{1}{4}\gamma^3 + \mathcal{O}(\gamma^5) \right), \quad b = \frac{1}{\epsilon} \left( -\frac{32}{\gamma^2} + 4 - \frac{3}{4}\gamma^2 + \mathcal{O}(\gamma^4) \right) \quad (\gamma \rightarrow 0).$$

This behaviour will induce very small-scale dynamics near the Takens-Bogdanov bifurcation for small  $\gamma$ , as we will see in the next section. At the other extreme, for large damping, we have

$$a = \frac{1}{\epsilon} \left( -\frac{2}{\gamma} - \frac{4}{\gamma^3} + \mathcal{O}\left(\frac{1}{\gamma^5}\right) \right), \quad b = \frac{1}{\epsilon} \left( -4 - \frac{4}{\gamma^2} + \mathcal{O}\left(\frac{1}{\gamma^4}\right) \right) \quad (\gamma \rightarrow \infty).$$

The unfolding theory of the Takens-Bogdanov bifurcation [16] tells us that in the Takens-Bogdanov singularity three codimension-one bifurcation curves meet in a quadratic tangency. Apart from the saddle-node and Hopf curves we already identified, this includes a curve of homoclinic bifurcations. We will encounter these homoclinic bifurcations in the next section.

Transcritical bifurcation: A second local codimension-two bifurcation occurs in our system when two saddle-node bifurcations coalesce. This transcritical bifurcation separates the two types of frequency-response curves shown in Figs. 1(a) and (b). The critical parameter values can be computed to be given by

$$\omega_{\text{TC}}^2 = \frac{1}{3} \left( 2 - \gamma^2 + \sqrt{1 - 4\gamma^2 + \gamma^4} \right), \quad \delta_{\text{TC}}^2 = \frac{\epsilon^2}{\gamma^2} \left( \omega_{\text{TC}}^6 + (\gamma^2 - 2)\omega_{\text{TC}}^4 + \omega_{\text{TC}}^2 \right), \quad (15)$$

while for the radius we have

$$r_{\text{TC}} = \frac{2\delta_{\text{TC}}}{1 + \omega_{\text{TC}}^2}. \quad (16)$$

One may verify that  $\omega_{\text{TC}} < 1$  and  $\delta_{\text{TC}} < \epsilon$  for all  $\gamma$  and  $\epsilon$ , while the radius of the corresponding fixed point satisfies  $r_{\text{TC}} > \epsilon > \delta_{\text{TC}}$ .

The eigenvalues at the transcritical bifurcation are

$$\lambda_1 = 0, \quad \lambda_2 = -\gamma, \quad \lambda_{3,4} = -\frac{1}{2}\gamma \pm i\frac{1}{2}\sqrt{10 - 3\gamma^2 + 2\sqrt{1 - 4\gamma^2 + \gamma^4}}.$$

The centre-manifold-reduced vector field (up to second order) reads

$$\dot{x} = ex^2, \quad (17)$$

where

$$e = \frac{-3z^7 + 16z^6 - 11z^5 - 40z^4 + 23z^3 + 24z^2 - 9z}{48\epsilon\gamma^2\omega_{\text{TC}}z^2(z+1)(z-3)^2}, \quad (18)$$

with

$$z = \omega_{\text{TC}}^2.$$

For small  $\gamma$  the coefficient  $e$  has the expansion

$$e = \frac{1}{\epsilon} \left( \frac{1}{12} + \frac{1}{96}\gamma^4 + \frac{1}{48}\gamma^6 + \mathcal{O}(\gamma^8) \right).$$

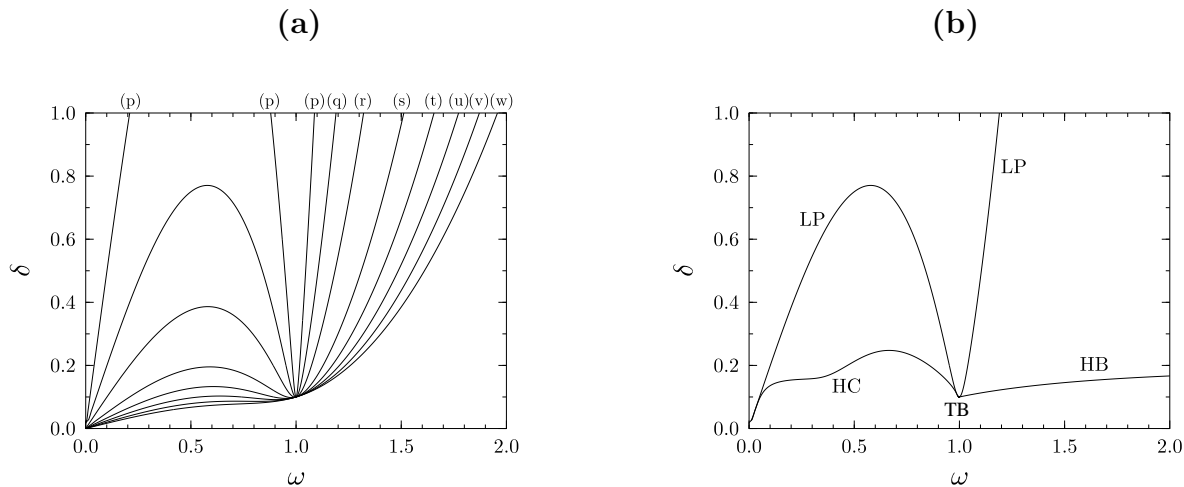


Figure 2: (a) Saddle-node lines for various values of  $\gamma$ ;  $\gamma = 0.02$  (p),  $0.05$  (q),  $0.1$  (r),  $0.2$  (s),  $0.3$  (t),  $0.4$  (u),  $0.5$  (v),  $0.6$  (w). (b) Parameter plane with bifurcation lines and eigenvalue configurations; LP: saddle-node bifurcations, HB: Hopf bifurcations, HC: homoclinic bifurcations. ( $\epsilon = 0.1$ ,  $\gamma = 0.05$ .)

The square-root in (15) becomes zero for  $\gamma = \gamma_0 := \sqrt{2 - \sqrt{3}} = 0.5176\dots$ . The corresponding codimension-three phenomenon is illustrated in Fig. 2(a) showing lines of saddle-node bifurcations for several values of  $\gamma$ . The transcritical bifurcations are represented by local minima of these saddle-node lines. For  $\gamma > \gamma_0$  local minima do not occur anymore, so we no longer have a transcritical bifurcation (the closed curve of fixed points for  $\delta > \delta_{TC}$  (cf. Fig. 1) has simply ceased to exist). The maxima of the saddle-node curves represent isola centres where closed curves of equilibria shrink to a point.

It can be checked that all curves in Fig. 2(a) pass through the point  $\omega = 1$ ,  $\delta = \epsilon$ . For these parameters  $r = 0$  is a solution of (4) and  $(x_1, x_2, x_3, x_4) = (0, 0, 0, 0)$  a, what could be called, ‘generalised solution’ of (1). The saddle-nodes for  $\omega > 1$  in Fig. 2(a) occur for negative  $r$  and are, hence, non-physical.

Summarising the bifurcation analysis of this section, Fig. 2(b) shows a typical  $\omega$ - $\delta$  parameter plane for not too large damping, with lines of codimension-one bifurcations meeting in codimension-two points, although the scale is such that the precise interaction of curves near TB is not clear. It is interesting to note that as  $\gamma \rightarrow 0$  we have  $\omega_{TB}, \omega_{TC} \rightarrow 1$  and  $\delta_{TB}, \delta_{TC} \rightarrow \epsilon$ . So, both codimension-two bifurcations in the dissipative system can be regarded to spring from the principal singularity at  $(\omega, \delta) = (1, \epsilon)$  of the conservative system.

For later reference the line of homoclinic bifurcations associated with the Takens-Bogdanov bifurcation has already been included in Fig. 2(b). The complicated dynamics near it will be the subject of the next section. There, we will also resolve the exact location of bifurcation lines near the Takens-Bogdanov bifurcation.

## 3 Global analysis

### 3.1 The case of large damping

We take  $\gamma = 2$  and show the sequence of bifurcations occurring near the Takens-Bogdanov bifurcation, the organising centre of the system's dynamics. Recall that for this value of  $\gamma$  there is no closed curve of fixed points. The Takens-Bogdanov bifurcation occurs at  $\omega_{\text{TB}} = 0.577350$ ,  $\delta_{\text{TB}} = 0.0384900$ , and the normal form coefficients are

$$a = -160/9 = -17.777778, \quad b = -640/9 = -71.111111. \quad (19)$$

For  $\delta = 0.04$  we have two branches of periodic solutions emanating from the fixed point curve, as shown in Fig. 3(b). In this figure, and in many figures to come, 'L<sup>2</sup>-norm' denotes the quantity  $\frac{1}{\sqrt{T}} \left( \int_0^T \sum_{i=1}^4 x_i^2(t) dt \right)^{1/2}$ , where  $T$  is the period of the periodic orbit. Note that for fixed  $T > 0$  this defines a genuine norm which reduces to the familiar  $(x_1^2 + x_2^2 + x_3^2 + x_4^2)^{1/2}$  in the case of a fixed point.

A short curve of periodic orbits runs from HB to HC on the lower, unstable branch of fixed points. Another one starts in a second HC point and runs off to small  $\omega$ . The Hopf bifurcation is subcritical, in agreement with the normal form analysis. Figs. 3(a)-(e) illustrate what happens to the curves of periodic orbits if the parameter  $\delta$  is increased. For  $\delta$  somewhere between 0.047 and 0.0471 the two curves meet and exchange branches. In the process an HC-HC connection is created which turns out to be too subtle to be detected. For slightly larger  $\delta$  the two HCs annihilate.

The above scenario is confirmed by the bifurcation curves in the  $\omega$ - $\delta$  diagram of Fig. 4, in which the HC curve was obtained by continuing very-high-period periodic solutions ( $T \approx 10000$ ). The maximum of the HC curve corresponds to the annihilation of the two HC bifurcations. At some point along the HC curve the homoclinic orbit changes from being repelling to being attracting, consistent with the series of plots in Fig. 3.

### 3.2 The case of moderate damping

The bifurcation picture in the large-damping case was rather simple. In particular, no complicated homoclinic phenomena and no chaotic motion was found. The moderate-damping case will prove to be much more complicated. To illustrate this we shall take  $\gamma = 0.05$ , the value which was used in [17]. The Takens-Bogdanov bifurcation has now moved to  $\omega_{\text{TB}} = 0.9996875000$ ,  $\delta_{\text{TB}} = 0.09994531952$ . For the present  $\gamma$  value we also have a transcritical bifurcation, very close to the Takens-Bogdanov bifurcation, located at  $\omega_{\text{TC}} = 0.9987476454$ ,  $\delta_{\text{TC}} = 0.09987492158$ . Associated with it is a closed curve of fixed points for values of  $\omega$  smaller than this critical value (cf. Fig. 1). The normal form coefficients for the Takens-Bogdanov bifurcation (14) have grown to

$$a = -1599.0003, \quad b = -127960.02, \quad (20)$$

while the coefficient (18) for the transcritical bifurcation is a modest

$$e = 0.83333399.$$

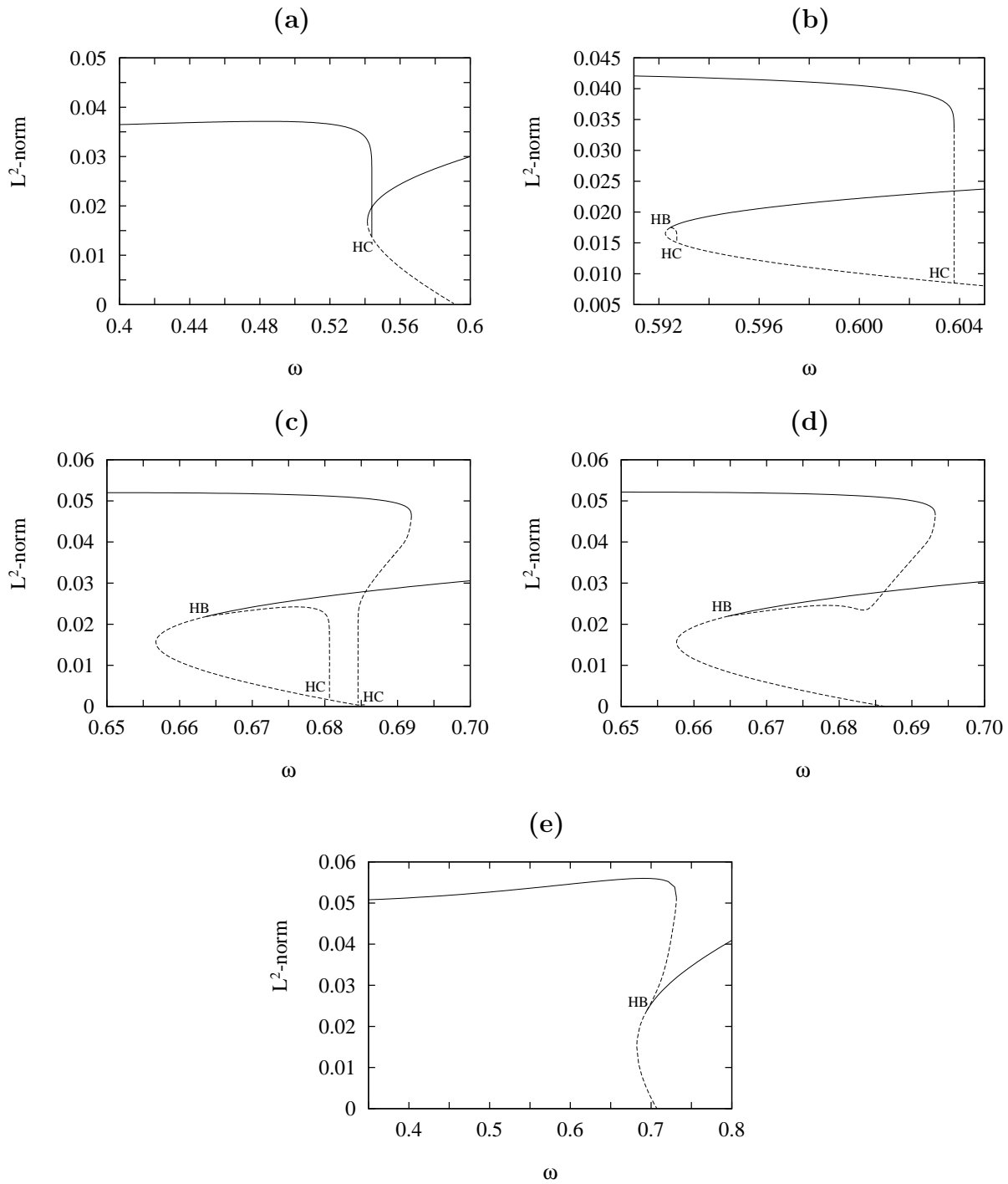


Figure 3: Bifurcation diagrams in the case of large damping showing curves of periodic solutions emanating from Hopf (HB) and homoclinic (HC) bifurcations of fixed points: (a)  $\delta = 0.035$ , (b)  $\delta = 0.04$ , (c)  $\delta = 0.047$ , (d)  $\delta = 0.0471$ , (e)  $\delta = 0.05$  ( $\epsilon = 0.1$ ,  $\gamma = 2$ ).

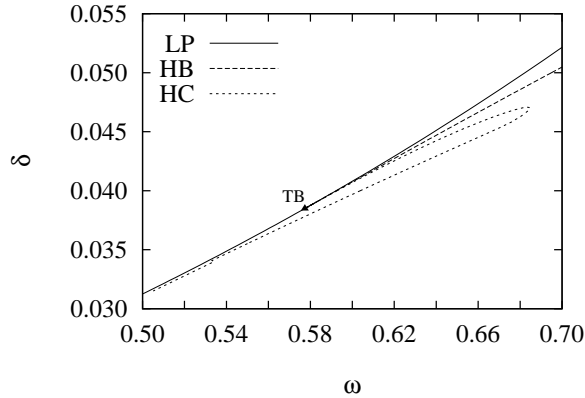


Figure 4: Bifurcation curves in the  $\omega$ - $\delta$  plane near the Takens-Bogdanov bifurcation, which is indicated by the black triangle ( $\epsilon = 0.1$ ,  $\gamma = 2$ ).

Although locally near TB we have to anticipate the same bifurcation phenomena as for the large-damping case, due to the large values of  $a$  and  $b$ , the bifurcation behaviour is rather more subtle. So subtle in fact that we had to hack the continuation code AUTO to give full 15-digit output in order to resolve the bifurcation structure. It is then seen that the HC curve in Fig. 2(b) makes a very small-scale fold just as it did for the large-damping case in Fig. 4. In a series of ‘snapshots’, i.e., for a number of values of the secondary bifurcation parameter  $\delta$ , we will now map out the global bifurcation structure of our system.

Because the Takens-Bogdanov bifurcation acts as the organising centre of the dynamics, we start with  $\delta$  close to  $\delta_{\text{TB}}$ . For  $\delta = 0.0999453198$ , which is slightly larger than  $\delta_{\text{TB}}$ , we find the situation depicted in Fig. 5(a), showing a curve of periodic solutions running from a subcritical Hopf bifurcation to a homoclinic bifurcation, analogous to the situation in Fig. 3(b). Note the ridiculously small scale on which phenomena take place: the parameter  $\omega$  varies only in the 14th digit! (We should remark that in the bifurcation diagrams among the Figs. 5-10 we have temporarily departed from our convention to signify branches of unstable solutions by broken lines.)

For slightly larger  $\delta$ , at  $\delta = 0.0999455$ , the situation is as shown in Fig. 5(b). The Hopf bifurcation has become supercritical, i.e., the coefficient  $c$  in (10) has changed sign, as is confirmed by the numerically obtained values listed in Table 1. At the change of stability, the transversality condition (9) was found to be satisfied with  $\alpha'_1(\omega_{\text{Hopf}}) = -6.21060878 \times 10^8$ . We observe that the emanating branch of periodic solutions is developing a wiggly ‘tower’. Period-doubling and subsequent reverse period-doubling bifurcations occur along the wiggles. At  $\delta = 0.09995$  (see Fig. 6(a)) the tower has grown to a considerable height but the curve of periodic solutions still ends in a homoclinic bifurcation on the lower branch of fixed points.

For the same parameter values there is a second homoclinic bifurcation on this branch, as there was in Figs. 3(b) and (c), from which a second branch of periodic solutions emanates. This branch connects to another homoclinic bifurcation located on the closed curve of fixed points at smaller  $\omega$ -values, see Fig. 6(b) (recall that for large damping, there not being this closed curve of fixed points, the curve of periodic solutions extends all the way down to  $\omega = 0$ ;

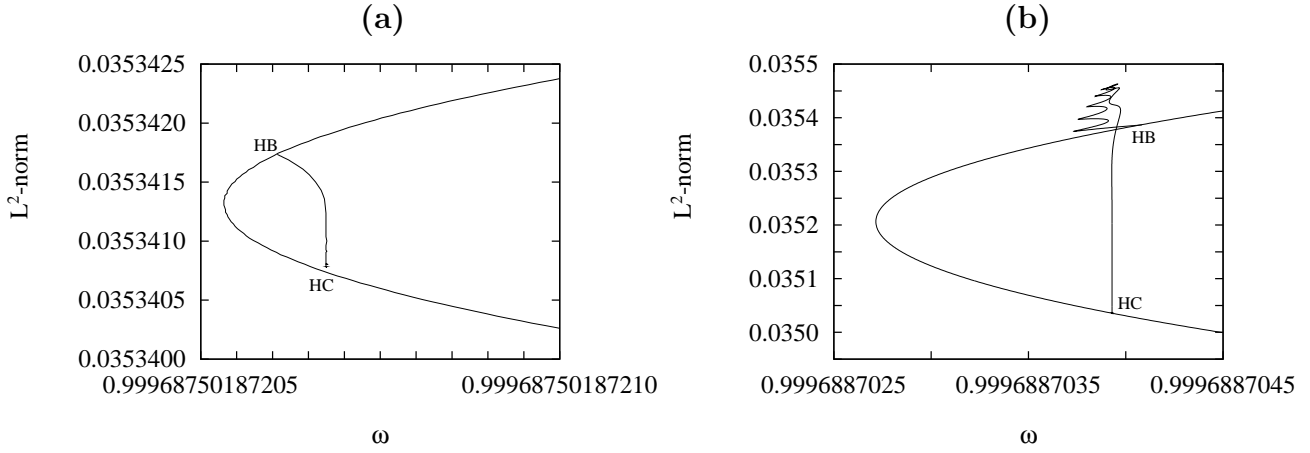


Figure 5: Bifurcation diagrams for  $\delta = 0.0999453198$  (a) and  $\delta = 0.0999455$  (b) ( $\epsilon = 0.1$ ,  $\gamma = 0.05$ ).

$\delta_{\text{HB}}$	$\omega_{\text{HB}}$	$c$
0.09994532	0.9996875032057	$2.767820318 \times 10^{13}$
0.0999453272	0.9996875512202	$9.858869311 \times 10^8$
0.099945327488	0.9996875531409	$5.519530491 \times 10^5$
0.099945327488138	0.99968755314179140	$3.299493631 \times 10^2$
0.099945327488138566	0.999687553141795176490	$3.657390931 \times 10^0$
0.099945327488138567	0.999687553141795183159	$-3.261661252 \times 10^{-1}$
0.099945327488139	0.99968755314179807	$-2.520554713 \times 10^2$
0.099945327489	0.9996875531475	$-3.432965759 \times 10^6$
0.099945328	0.9996875565554	$-2.497274757 \times 10^9$
0.09994533	0.9996875698937	$-1.75053129 \times 10^{10}$

Table 1: Parameters  $\delta$  and  $\omega$  and the normal form coefficient  $c$  at Hopf bifurcation, signalling a very rapid transition from a subcritical to a supercritical bifurcation ( $\epsilon = 0.1$ ,  $\gamma = 0.05$ ).

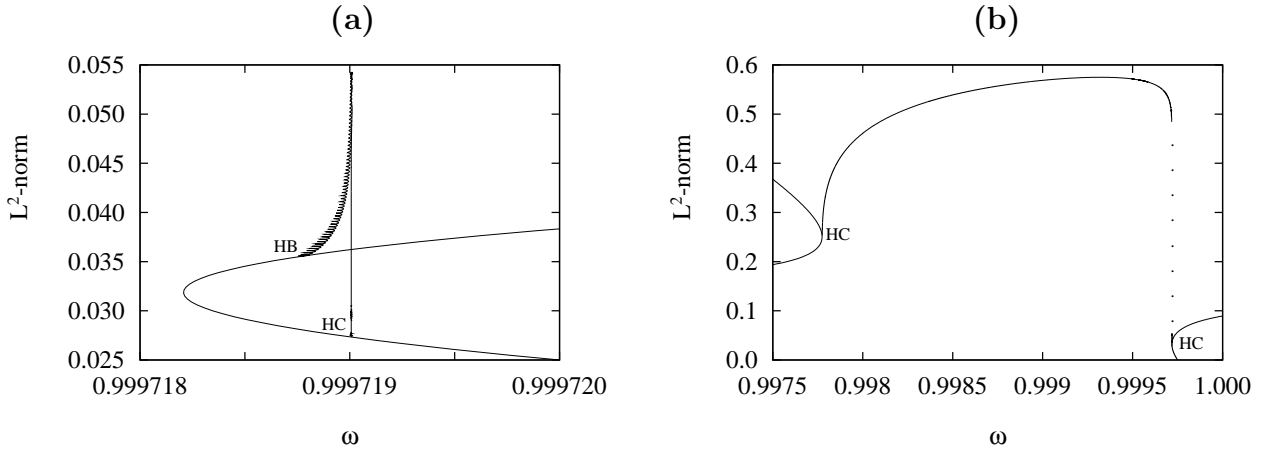


Figure 6: Bifurcation diagrams for  $\delta = 0.09995$  ( $\epsilon = 0.1$ ,  $\gamma = 0.05$ ).

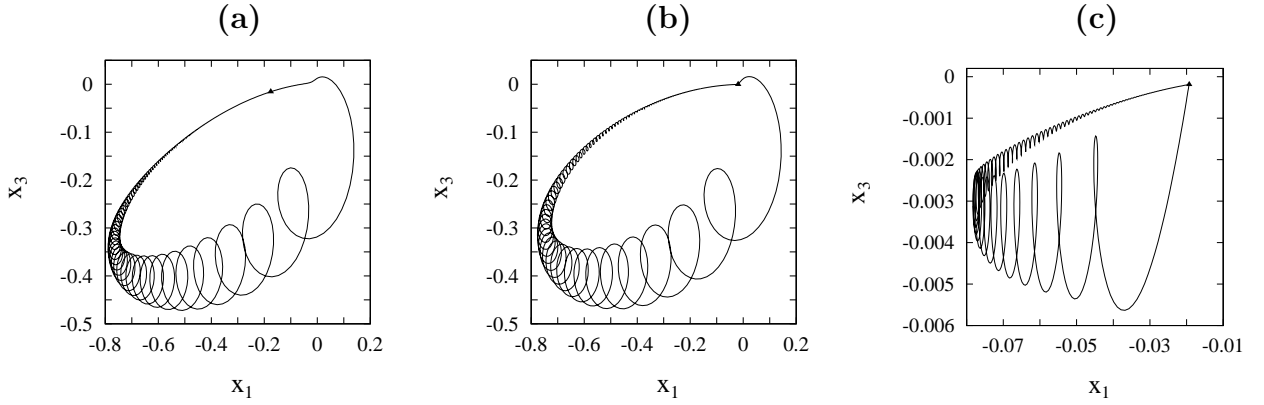


Figure 7: (Approximations to) homoclinic orbits for  $\delta = 0.09995$ : (a)  $\omega = 0.99777903$  ( $T = 10000$ ), (b)  $\omega = 0.99971898$  ( $T = 772$ ), (c)  $\omega = 0.99971901$  ( $T = 10000$ ) ( $\epsilon = 0.1$ ,  $\gamma = 0.05$ ).

cf. Fig. 3). Note the difference in scale of both curves of periodic solutions: the tower of Fig. 6(a) is included in Fig. 6(b) but is barely visible. Approximations of the three homoclinic orbits present in Fig. 6(b) (in fact, periodic orbits of very high period) are shown in Fig. 7. The orbit in Fig. 7(a) is associated with a saddle-focus-type fixed point on the low-frequency branch. The eigenvalues are

$$\rho \pm i\omega = -0.02500 \pm i 1.8503, \quad \lambda = -0.05007, \quad \nu = 0.00007303, \quad (21)$$

where  $\nu$  is very small owing to the fact that we are very close to a saddle-node bifurcation. As a result, near the fixed point the ratio between attraction in one direction and repulsion in the other, as expressed by Šil'nikov's number  $\sigma := -\rho/\nu$ , is larger than 1 and we generically have a so-called 'tame' Šil'nikov bifurcation [6]. The corresponding homoclinic orbit is attracting. The fixed points associated with the homoclinic orbits of Figs. 7(b) and (c) have real eigenvalues.

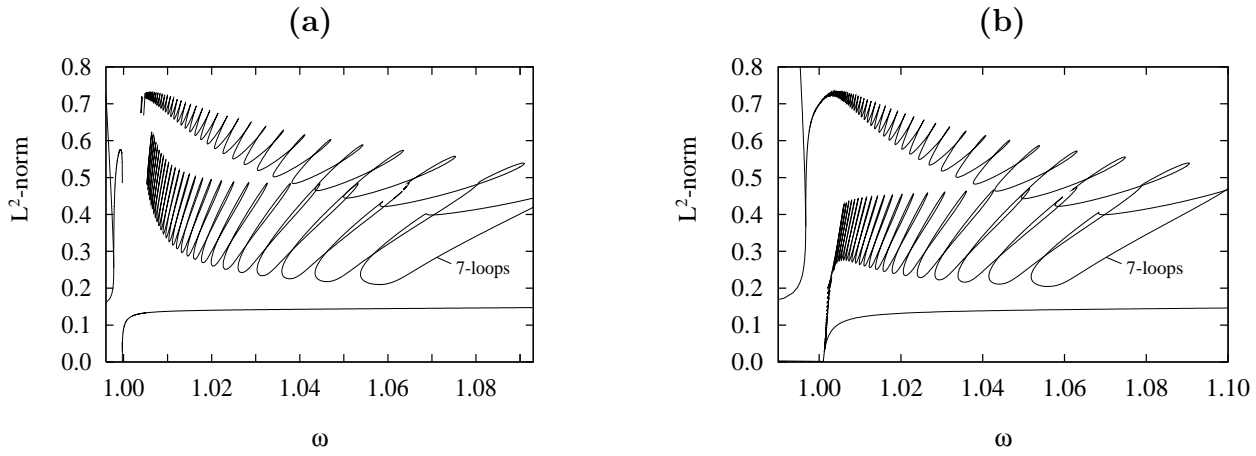


Figure 8: Bifurcation diagrams for  $\delta = 0.09995$  (a) and  $\delta = 0.1002$  (b) ( $\epsilon = 0.1$ ,  $\gamma = 0.05$ ).

There is yet another structure of periodic solutions present at  $\delta = 0.09995$ . It is given in Fig. 8(a) along with the previous two (although now the tower is not visible anymore). It consists of two connected wiggly curves of alternately stable and unstable solutions lying next to each other. On each of the stable branches there are period-doubling and subsequent reverse period-doubling bifurcations. The behaviour of this structure upon decrease of  $\delta$  bears a striking resemblance to the action of a zipper: opposite strands of solutions line up, connect and exchange branches in transcritical bifurcations, thus shedding a closed curve (isola) of periodic orbits. Solutions on a particular isola all look similar when plotted in  $x_1$ - $x_3$  diagrams, even though different parts of the curve originate from different strands of the zipper. Clearly, there must be an underlying mechanism responsible for this synchronisation.

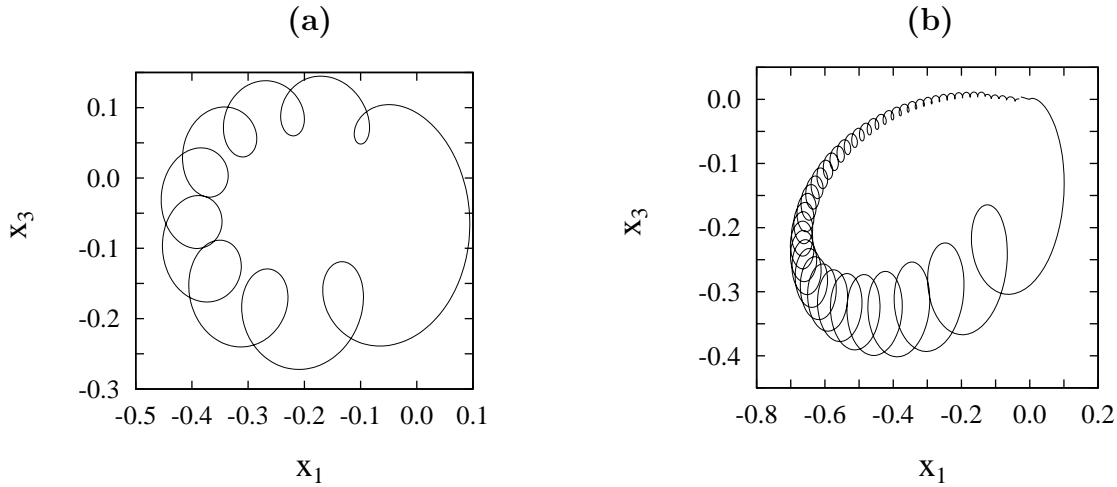


Figure 9: Periodic solutions on isolae present in Fig. 8(a): (a) 8-loop at  $\omega = 1.07$  ( $T = 29.406859$ ), (b) 45-loop at  $\omega = 1.003978$  ( $T = 157$ ) ( $\epsilon = 0.1$ ,  $\gamma = 0.05$ ,  $\delta = 0.09995$ ).

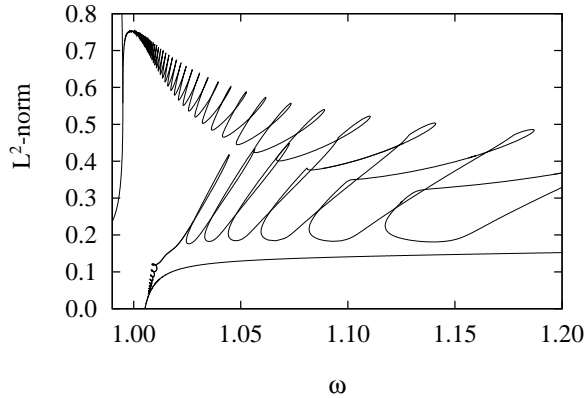


Figure 10: Bifurcation diagram for  $\delta = 0.101$  ( $\epsilon = 0.1$ ,  $\gamma = 0.05$ ).

Specifically, the periodic orbits are of a type called  $n$ -loops in [17], because their  $x_1$ - $x_3$  projections form a number,  $n$ , of small loops before closing up. For instance, the just detached closed curve of periodic solutions in Fig. 8(a) consists of 8-loops (see Fig. 9). To the right of it we have a 7-loop isola also shown in Fig. 8(a). Isolae of  $n$ -loops with  $1 \leq n \leq 6$  exist for larger values of  $\omega$  but are not shown in Fig. 8(a) (but see Fig. 11).

A similar process of  $n$ -loop isolation occurs at the small- $\omega$  end of the bi-wiggly structure. A small closed curve of periodic solutions can be seen in Fig. 8(a). It actually consists of 45-loops an example of which is given in Fig. 9. We would expect the bi-wiggly structure to form a closed curve itself, but towards the small- $\omega$  end convergence problems were experienced during the numerical continuation (look ahead, though, to Fig. 17, where such problems do not occur). We should remark that for periodic orbits with a large number of loops the number  $n$  may be slightly ambiguous. In [17] it was shown, however, that in the limit  $\delta \rightarrow 0$  the labelling can be made rigorous.

Upon further increase of  $\delta$  the tower rises very rapidly until it collides with the zipper. At about the same instant the homoclinic arc hits the zipper from the left. Thus at  $\delta = 0.1002$  we have the bifurcation diagram depicted in Fig. 8(b) showing a curve of periodic orbits emerging from the Hopf bifurcation and terminating in the homoclinic bifurcation on the left-hand branch of fixed points. Additionally, we still have a number of closed curves of solutions. Increasing  $\delta$  these isolae are opened up upon contact with the zipper. In Fig. 8(b) the 8-loop isola is about to be split and made part of the wiggly structure.

At  $\delta = 0.101$  (Fig. 10) this has happened. At the same time we observe that the lower strand of the zipper loses its wiggles through interaction with the lower wiggly curve that previously formed the tower. This process of repeating exchanges of solution branches is not unlike the action of the zipper and also involves the formation of isolae of periodic orbits. These seem to be very ‘short-lived’, however, quickly shrinking down to zero upon variation of  $\delta$ . When the lower strand has lost all its wiggles the former tower takes over to interact with the upper strand of the zipper to ‘catch’ the remaining  $n$ -loop isolae. As an example, Fig. 11, in a series of snapshots, shows how the last closed curve of 1-loops gets included in the wiggly structure.

The next stop on our journey is at  $\delta = 0.2$ , the central value in our earlier work [17]. The

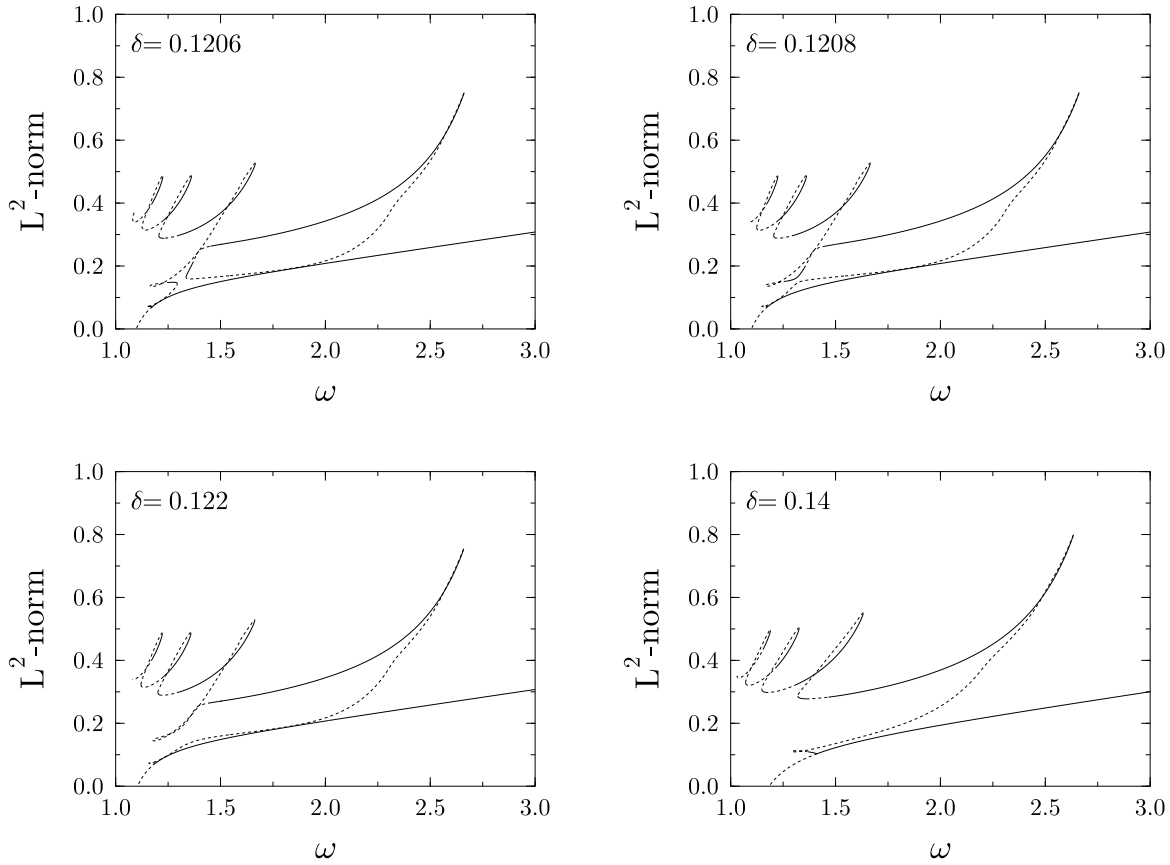


Figure 11: Bifurcation diagrams for four values of  $\delta$  illustrating the inclusion of the last isola of periodic orbits (1-loops) in the wiggly curve ( $\epsilon = 0.1$ ,  $\gamma = 0.05$ ).

bifurcation diagram is given in Fig. 12. The Hopf bifurcation has moved to infinity (recall that  $\delta_{\text{Hopf}} \rightarrow 2\epsilon$  as  $\omega \rightarrow \infty$ ) and there are no isolae of periodic solutions left. The homoclinic bifurcation, in the meantime, has become of chaotic Šil'nikov type, as confirmed by the eigenvalues of the corresponding fixed point which are

$$\rho \pm i\omega = -0.02500 \pm i 1.7537, \quad \lambda = -0.1362, \quad \nu = 0.08621, \quad (22)$$

yielding  $\sigma = -\rho/\nu < 1$ . Indeed, the wiggly curve has all the characteristics of the usual curve of periodic solutions associated with a chaotic Šil'nikov bifurcation [24]. Specifically, we have alternating stable and unstable branches with on each of the stable branches period-doubling and subsequent reverse period-doubling bifurcations. Also, the period of the periodic orbits diverges upon approaching the homoclinic bifurcation, as illustrated by the period curve in Fig. 12(b). Fig. 13 shows (projections of) the fundamental periodic solution and solutions along the first three wiggles (counted from the right) in Fig. 12. The closer  $\omega$  is to the homoclinic bifurcation value the more loops occur.

Quantitative evidence for a chaotic Šil'nikov bifurcation can be obtained from an inspection

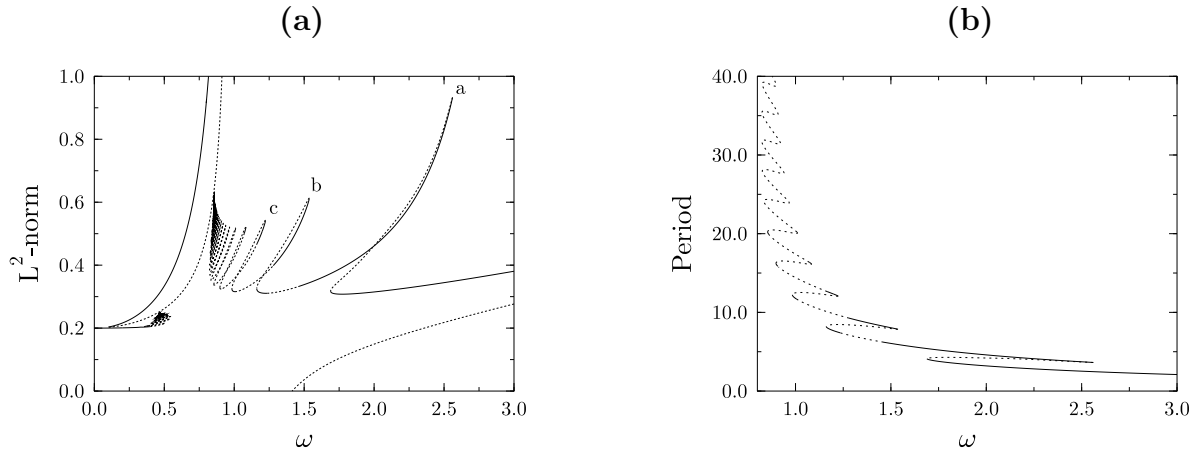


Figure 12: (a) Wiggly curve of periodic solutions ending in a chaotic Šil'nikov bifurcation; 'a', 'b' and 'c' denote 1-loop, 2-loop and 3-loop branches, respectively. (b) Period curve. ( $\delta = 0.2$ ,  $\epsilon = 0.1$ ,  $\gamma = 0.05$ .)

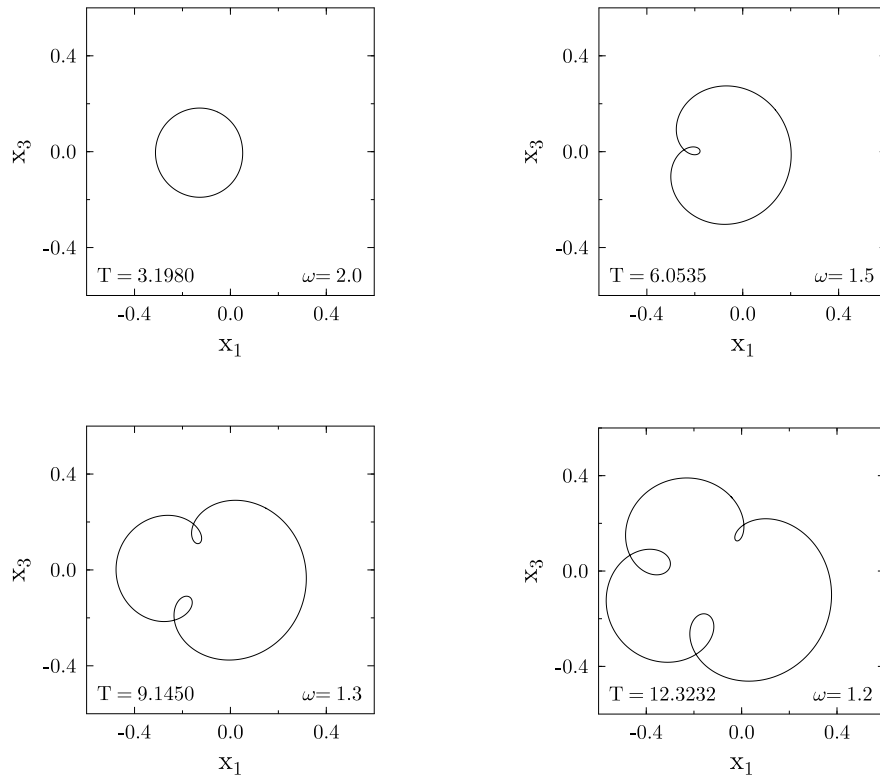


Figure 13: Stable period solutions – the fundamental solution and the first three  $n$ -loops – along the wiggly curve in Fig. 12;  $T$  denotes their period ( $\delta = 0.2$ ,  $\epsilon = 0.1$ ,  $\gamma = 0.05$ ).

of the asymptotic properties of the wiggly curve in Fig. 12. The asymptotic ratio of parameters at which saddle-node bifurcations occur is completely determined by the complex eigenvalues of the fixed point (cf. [24]):

$$\lim_{i \rightarrow \infty} \frac{\mu_{i+1}}{\mu_i} = -\exp \frac{\rho\pi}{\omega} = -0.9562, \quad (23)$$

where we have used (22). A direct calculation of this ratio, using the numerically determined parameter values at which saddle-node bifurcations occur, gives a limiting value of  $-0.956 \pm 0.002$ , in agreement with (23). This relatively large value (due to the low damping in the system) explains why the wiggles damp out so slowly in Fig. 12, and why so many bifurcations along the curve can be detected numerically.

The transition from a tame ( $\sigma > 1$ ) to a chaotic ( $\sigma < 1$ ) Šil'nikov bifurcation occurs at a codimension-two homoclinic bifurcation along the line HC in Fig. 2(b) (see also Fig. 18). In a three-dimensional setting this bifurcation has been studied by Belyakov [5] (see [6] for a review).

**Period-doubling cascades.** From the period-doubling bifurcation points on the curve in Fig. 12(a) branches of periodic solutions emanate which undergo further period-doubling bifurcations. Numerical work suggests full period-doubling cascades, followed by reverse cascades which restabilise the initial periodic solutions. For example, by checking the Floquet multipliers, the first seven period-doublings on the 1-loop branch in Fig. 12(a) are found to occur at  $\omega_1=1.458128$ ,  $\omega_2=1.441673$ ,  $\omega_3=1.438840$ ,  $\omega_4=1.438322$ ,  $\omega_5=1.438219$ ,  $\omega_6=1.438196$ ,  $\omega_7=1.438192$ . Defining  $\delta_i = (\omega_{i-1} - \omega_{i-2})/(\omega_i - \omega_{i-1})$  we have the following sequence

$$\begin{aligned} \delta_3 &= 5.808 \pm 0.002 \\ \delta_4 &= 5.469 \pm 0.012 \\ \delta_5 &= 5.03 \pm 0.06 \\ \delta_6 &= 4.5 \pm 0.2, \end{aligned}$$

showing good agreement with the theory of one-dimensional mappings [8, 13] which predicts that the  $\delta_i$  converge geometrically to the universal Feigenbaum constant  $\delta_F = 4.6692\dots$  as  $i \rightarrow \infty$ .

Extrapolating the sequence, one expects the accumulation point to be located at  $\omega_\infty = 1.438191$ . For slightly smaller  $\omega$  a chaotic attractor is found (see the phase-space plot in Fig. 14). The  $\omega$ -window where this attractor exists seems to be very narrow as already for  $\omega=1.4380$  we are left with only transient chaos, the system eventually relaxing to a stable once-period-doubled solution.

Other Šil'nikov-type chaotic attractors are found after other period-doubling cascades along the wiggly curve of Fig. 12(a).

**Homoclinic collision.** For  $\delta = 0.2$  there is a second chaotic Šil'nikov bifurcation at  $\omega = 0.4676$ . The associated wiggly curve is visible for small frequencies in Fig. 12(a). Note that the existence of two homoclinic bifurcations for  $\delta = 0.2$  is consistent with the HC-curve in Fig. 2(b) which has a local maximum for  $(\omega, \delta) = (0.6642, 0.2476)$ . If  $\delta$  is decreased the second Šil'nikov bifurcation quickly recedes to small  $\omega$  and the associated periodic solutions soon become undetectable.

Increasing  $\delta$  beyond the current value of 0.2 both homoclinic bifurcations on the fixed point curve move towards each other, their associated wiggly curves first clashing at  $\delta \simeq 0.219$ . In Fig. 15 solution curves are shown just before and just after this collision. In the latter case a

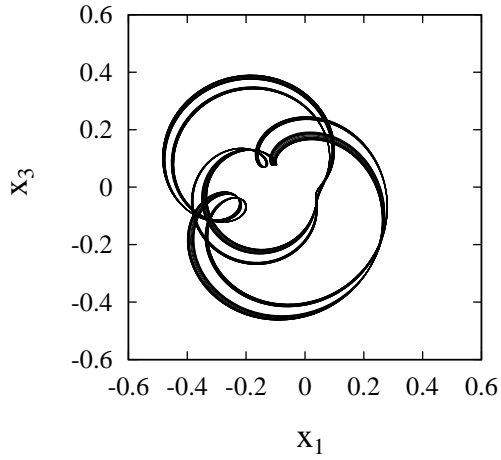


Figure 14: Phase-space projection of a chaotic attractor along the 1-loop branch ( $\epsilon = 0.1$ ,  $\gamma = 0.05$ ,  $\delta = 0.2$ ,  $\omega = 1.43805$ ).

bi-wiggly curve of periodic solutions connects the two homoclinic bifurcation points. There is also an isola of periodic solutions formed by the interaction of branches of the wiggly curves. Presumably, a few more of such closed curves exist as there seems to be a gap between the bi-wiggly curve and the lower solution branches.

The homoclinic bifurcations eventually disappear at  $\delta = 0.2476$ . What is left is a branch of periodic solutions for all frequencies. Further increasing  $\delta$  the wiggles with different coexisting periodic solutions (cf. Fig. 13) gradually disappear in cusp bifurcations in which two saddle-nodes coalesce. Fig. 16 shows the situation for  $\delta = 1.5$ . Only the primary wiggle with 1-loop solutions has survived. Eventually, this branch will also disappear in a cusp at  $\delta \simeq 8.0$ . What remains is a ‘background’ curve of nearly-circular fundamental periodic solutions (compare the

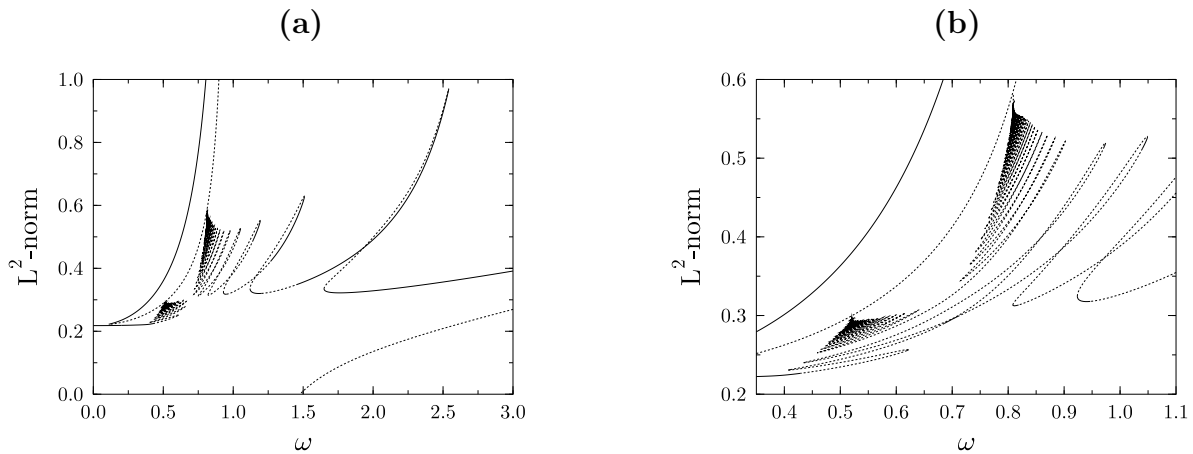


Figure 15: Homoclinic collision: (a)  $\delta = 0.218$ , (b)  $\delta = 0.22$  ( $\epsilon = 0.1$ ,  $\gamma = 0.05$ ).

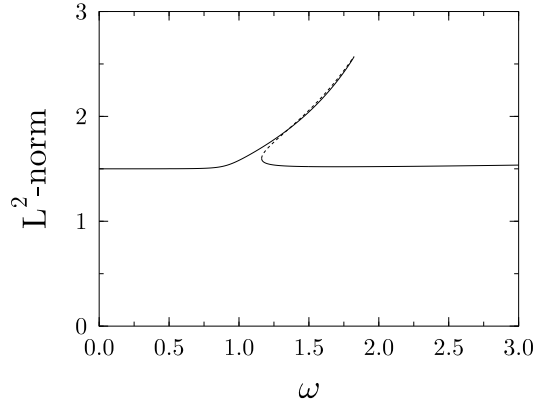


Figure 16: The last surviving wiggle of 1-loops ( $\epsilon = 0.1$ ,  $\gamma = 0.05$ ,  $\delta = 1.5$ ).

orbit drawn in Fig. 13(a)).

As a final stage of our journey let us decrease  $\delta$  below  $\delta_{\text{TB}}$ . Then there is no Hopf bifurcation and no tower of periodic solutions. The arc of periodic solutions running between two homoclinic bifurcations, as in Fig. 6(b), at first still exists but upon further decrease of  $\delta$  disappears as the two homoclinic bifurcations annihilate. For this to happen the two homoclinic bifurcations must be on the same branch of fixed points, so we must have  $\delta < \delta_{\text{TC}}$ . For even lower  $\delta$  we no longer have homoclinic bifurcations and the zipper constitutes the only source of periodic solutions. As an example, Fig. 17 shows the situation for  $\delta = 0.099$ . We observe a central structure comprising the eight  $n$ -loops with  $13 \leq n \leq 20$ , while all other  $n$ -loops with either larger or smaller  $n$  have already detached (two flanking examples are included in Fig. 17).

Further reducing  $\delta$ , all  $n$ -loops detach and continue living on closed bifurcation curves. Here,

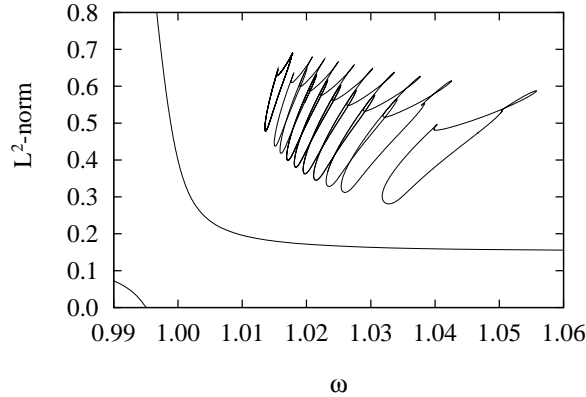


Figure 17: Bifurcation diagram for  $\delta = 0.099$  showing 8  $n$ -loops ( $13 \leq n \leq 20$ ) still zipped up while all others (of which two are shown) have been freed. ( $\epsilon = 0.1$ ,  $\gamma = 0.05$ ).

we enter the mode-locking regime studied in [17] and summarised in the next section. In the  $\omega$ - $\delta$  diagram the  $n$ -loops now exist between two saddle-node lines forming the boundaries of resonance tongues.

## 4 Mode-locking

Continuation of saddle-node bifurcations of the first six  $n$ -loops yields the resonance tongues of Fig. 18. Note that the tongues do not actually emerge from the  $\omega$  axis. This depends on how we scale the parameters of the system. If we were to take  $\gamma = \bar{\gamma}\delta$ , i.e., if we let the damping go to zero with the nonlinearity  $\delta$ , then we would find that for  $n = 1, 2$  and  $3$  the tongues would touch the horizontal axis in Fig. 18 (see Fig. 19). Taking the quadratic scaling  $\gamma = \bar{\gamma}\delta^2$  would also connect the tongues for  $n = 4, 5$  and  $6$ , etc.

The combined curves of saddle-node bifurcations summarise many of the bifurcations seen in the bifurcation diagrams of the previous section. In particular, note the pair of cusp points (one for relatively high, the other for relatively low  $\delta$ ) for each of the  $n$ -loops, where wiggles of periodic solutions disappear (cf. (16)). (Recall from the previous section that the 1-loop tongue has a cusp well outside the present plot at  $\delta \simeq 8.0$ .) We should remark, however, that Fig. 18 does not give a complete account of the bifurcation structure associated with the  $n$ -loops. For instance, (cascades of) period-doubling lines are known to exist in each of the resonance regions but have not been drawn in. At the end points of the curves of saddle-nodes just beyond the lower cusps the numerical continuation breaks down due to convergence problems whose cause remains unclear.

It was shown in [17] that for a better understanding of the resonance nature of the  $n$ -loops it is useful to return to the unreduced system (2). The unperturbed version ( $\delta = 0$ ) of it represents a driven pair of linear oscillators and the resonances can be described in terms of three-frequency mode-locking, one of the frequencies being the forcing frequency  $\omega$ . In the unreduced system, the  $n$ -loops correspond to quasi-periodic motions (on 2-tori) in partial mode-locking, i.e., with one rational relation present between the three frequencies. This situation is only structurally stable within the class of rotationally symmetric vector fields. As was shown in [17], a perturbation destroying this symmetry might result in a second resonance relation being established between the frequencies, leading to fully mode-locked periodic motion (i.e., a further mode-locking on the already mode-locked invariant 2-tori).

The three-frequency mode-locking viewpoint in [17] allowed us to derive, by semi-analytical means, that the  $n$ -loop resonance tongues emerge from the frequency axis at

$$\omega_{0,n} = 1 + \frac{2}{n} \quad (n = 1, 2, 3, \dots), \quad (24)$$

A further result was that the emerging  $n$ -loop has period

$$T_{0,n} = n\pi. \quad (25)$$

Note that unlike in the case of circle maps, different orders of resonance can evolve into each other. Indeed, the zipper structure of the previous section constitutes a global connection between different  $n$ -loops.

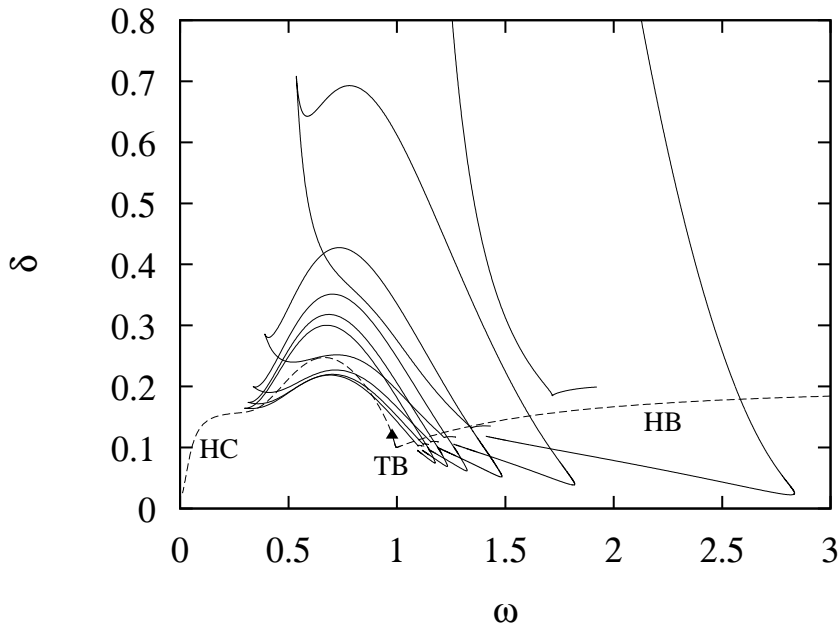


Figure 18: Resonance tongues for (1). Tongue boundaries are formed by saddle-node curves for the  $n$ -loop periodic orbits. Also shown are lines of Hopf (HB) and homoclinic (HC) bifurcations of the fixed point. The solid triangle indicates the codimension-two homoclinic bifurcation point  $(\omega, \delta) = (0.981, 0.117)$ , where the Šil'nikov number  $\sigma$  becomes 1. ( $\epsilon = 0.1$ ,  $\gamma = 0.05$ .)

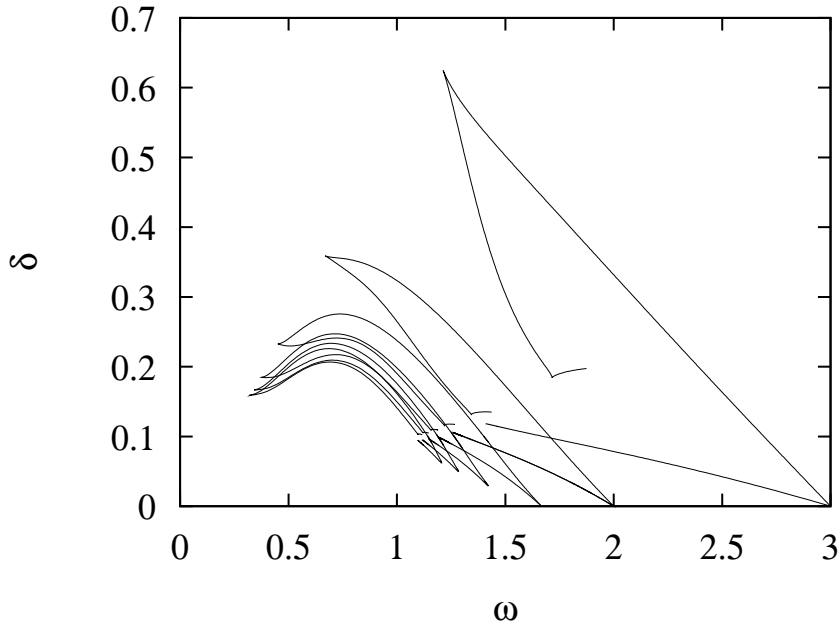


Figure 19: Resonance tongues for (1) taking  $\gamma = \bar{\gamma}\delta$ . Tongue boundaries are formed by saddle-node curves for the  $n$ -loop periodic orbits. ( $\epsilon = 0.1$ ,  $\bar{\gamma} = 0.5$ .)

## 5 Discussion

This paper has presented new sequences of transcritical bifurcations of periodic solutions in the interaction of resonances in an autonomous four-dimensional system. The system is a reduced version of a rotationally symmetric driven system of two coupled oscillators. The resonances of the system are best understood on the level of the original unreduced system in which the periodic orbits correspond to invariant tori.

Although our results have been obtained for a particular equation, we conjecture that the same type of behaviour occurs in a more general class of systems. The synchronised action of the zipper (see, e.g., Fig. 8), in particular, suggests an underlying governing mechanism. It would be useful to try and write down an abstract mathematical model of this behaviour. In this respect we remark that the zipping up of resonance tongues found in our system is reminiscent of the ‘merging of resonance tongues’ reported in [21], where also Šil’nikov bifurcations are involved. In [21] the system is an autonomous three-dimensional system which is an unfolding of the truncated normal form of a saddle-node/Hopf bifurcation (see also [22]). Similar behaviour has also been observed in an unfolding of the pitchfork/Hopf bifurcation [18]. The origin of the resonances in both these systems is different from that in our system, being associated with a secondary Hopf bifurcation.

It is worth mentioning here that recent work by Champneys & Rodríguez-Luis [7] shows how a collision of two Šil’nikov-type homoclinic orbits can lead to the destruction of wiggly curves by the formation of isolae of periodic solutions. This scenario would seem to apply to our homoclinic collision occurring at relatively large  $\delta$  (see Fig. 15). Our zipper, however, occurs at smaller  $\delta$  (cf. Fig. 8) where it cannot be related to a degenerate Šil’nikov bifurcation, and hence a different mechanism must be responsible.

In the previous sections we have used  $\omega$  and  $\delta$  as bifurcation parameters. In order to explore possible higher-order bifurcation phenomena we will now introduce the damping coefficient  $\gamma$  as a third bifurcation parameter. First note that in the conservative limit ( $\gamma \rightarrow 0$ ) the two codimension-two points discussed in Section 2 (cf. Fig. 2(b)) merge at  $(\omega, \delta) = (1, \epsilon)$ . The corresponding fixed points, however, remain different: from (12) and (13) we see that for the Takens-Bogdanov point we have  $r \rightarrow \epsilon/4$ , while for the transcritical bifurcation point Eqs. (15) and (16) give  $r \rightarrow \epsilon$ .

Indeed, for  $(\omega, \delta, \gamma) = (1, \epsilon, 0)$  system (1) has a degenerate one-parameter set of fixed points given by

$$x_1 = -r, \quad x_2 = 0, \quad x_3 = 0, \quad x_4 = -r, \quad (r \in \mathbb{R}^+). \quad (26)$$

The linearised vector field at these fixed points (26) reads

$$A_r = \begin{pmatrix} 0 & 1 & 1 & 0 \\ -1 & 0 & 0 & 1 \\ -1 & 0 & 0 & 1 \\ 0 & -1 & (\epsilon - r)/r & 0 \end{pmatrix}. \quad (27)$$

The Jordan canonical form of  $A_r$  is

$$J_r = \begin{pmatrix} 0 & 1 & 0 & 0 \\ 0 & 0 & 0 & 0 \\ 0 & 0 & \alpha & 0 \\ 0 & 0 & 0 & \alpha \end{pmatrix}, \quad \text{where} \quad \alpha = \sqrt{\frac{\epsilon}{r} - 4}. \quad (28)$$

We conclude that for  $r > \epsilon/4$  we have a (degenerate) codimension-three Takens-Bogdanov/Hopf bifurcation, while for  $r < \epsilon/4$  we have just a Takens-Bogdanov bifurcation. For  $r = \epsilon/4$ , the end point of our line of Takens-Bogdanov bifurcations when continued in  $\gamma$ , we have the Jordan form

$$J = \begin{pmatrix} 0 & 1 & 0 & 0 \\ 0 & 0 & 1 & 0 \\ 0 & 0 & 0 & 1 \\ 0 & 0 & 0 & 0 \end{pmatrix}, \quad (29)$$

which represents a singularity of codimension four.

A full unfolding of the codimension-four singularity (29) can, of course, not be accomplished in a three-parameter family of vector fields. Indeed, it is because of the one-parameter family of fixed points (26), effectively giving us a fourth bifurcation parameter  $r$ , that we are able to arrive at the codimension-four singularity in the first place. Nevertheless, complicated dynamics can be anticipated near the singularity (29). Note in this respect that the wiggles of periodic solutions (as for instance in Fig. 12) damp out ever more slowly as  $\gamma$  is decreased (cf. Fig. 23).

We also observe from (24) that we have an accumulation of resonance tongues in Fig. 18 with limiting frequency  $\omega = 1$ .

It is interesting to note that the divergence of the Takens-Bogdanov normal form coefficients  $a$  and  $b$  (14) as the codimension-four singularity is approached, has also been observed for reversible Takens-Bogdanov normal form coefficients in the approach of the same singularity (29) within the class of reversible vector fields (in which case (29) is of codimension two) [20]. In the reversible case the divergences could be suppressed by carefully rescaling the equations.

Finally, we make some comments which serve to relate the results of this paper to experimental work on rotor systems with clearances as reported in the literature. Complicated dynamics in such systems has been discussed by several authors. Ehrich [11] describes experiments on a high-speed turbomachine with bearing clearance, observing subharmonic vibrations with frequencies  $1/n$  times the forcing frequency (up to  $n = 8$ ), and transitions between them via period-doubling cascades and chaotic motion. Similar transitions have been reported in [12, 1, 14]. Qualitatively, this is exactly the type of behaviour to be expected in a system with mode-locking as studied in the present paper.

In Adiletta et al. [1] complicated motion is observed for intermediate values of the clearance parameter ( $\delta = 0.3 - 0.5$ ), with smaller and larger  $\delta$  predominantly giving rise to periodic responses. This is broadly consistent with our results. For a more quantitative comparison the paper by Gonsalves et al. [14] is especially useful since it describes experiments on a basic two-degrees-of-freedom rotor system concentrating on the effects of bearing clearance only, and also because it quotes all the relevant parameters. It reports complicated resonance behaviour, including chaotic motion, for a rotor with a linear damping coefficient  $\gamma = 0.17$ , a clearance equal to the eccentricity (i.e.,  $\delta = \epsilon$ ), and a dimensionless driving frequency  $\omega \simeq 2.5$ . These parameters are right in our region of complicated dynamics.

Although many of the dynamical features discussed in this paper are likely to be too subtle to be observed experimentally, it would be interesting to perform some careful experiments on a rotor system with bearing clearance with a particular focus on observing features associated with homoclinic behaviour, such as diverging periods of periodic solutions.

# Acknowledgements

I would like to thank Carlo Laing, then at Cambridge University, for bringing to my attention the work of Vivien Kirk. Thanks are also due to Alan Champneys for reading the manuscript. The present work was made possible by a European Union Human Capital and Mobility grant.

## References

- [1] Adiletta, G., Guido, A.R., Rossi, C., Chaotic motions of a rigid rotor in short journal bearings, *Nonlinear Dynamics* 10, 251-269 (1996).
- [2] Arnol'd, V.I., *Geometric Methods in the Theory of Ordinary Differential Equations* (Springer, New York, 1982).
- [3] Aronson, D.G., Chory, M.A., Hall, G.R., McGehee, R.P., Bifurcations from an invariant circle for two-parameter families of maps of the plane: a computer-assisted study, *Commun. Math. Phys.* 83, 303-354 (1982).
- [4] Baesens, C., Guckenheimer, J., Kim, S., MacKay, R.S., Three coupled oscillators: mode-locking, global bifurcations and toroidal chaos, *Physica* 49D, 387-475 (1991).
- [5] Belyakov, L.A., Bifurcation of systems with homoclinic curve of a saddle-focus with saddle quantity zero, *Math. Notes* 36, 838-843 (1984). (Originally published in *Mat. Zametki* 36(5), 681-689 (1984).)
- [6] Champneys, A.R. & Kuznetsov, Yu.A., Numerical detection and continuation of codimension-two homoclinic bifurcations, *Int. J. Bifurcation and Chaos* 4, 785-822 (1994).
- [7] Champneys, A.R. & Rodríguez-Luis, A.J., The non-transverse Shil'nikov-Hopf bifurcation: uncoupling of homoclinic orbits and homoclinic tangencies, submitted to *Physica D* (1997).
- [8] Collet, P. & Eckmann, J.-P., *Iterated Maps on the Interval as Dynamical Systems* (Birkhäuser, Basel, 1980).
- [9] Doedel, E.J., Champneys, A.R., Fairgrieve, T.F., Kuznetsov, Y.A., Sandstede, B. & Wang, X., *AUTO97: Continuation and Bifurcation Software for Ordinary Differential Equations* (1997).
- [10] Doedel, E.J., Keller, H.B. & Kernévez, J.P., Numerical analysis and control of bifurcation problems, *Int. J. Bifurcation and Chaos* 1, 493-520, 745-772 (1991).
- [11] Ehrich, F.F., Some observations of chaotic vibration phenomena in high-speed rotordynamics, *J. of Vibration and Acoustics* 113, 50-57 (1991).
- [12] Ehrich, F.F., Observations of subcritical superharmonic and chaotic response in rotordynamics, *J. of Vibration and Acoustics* 114, 93-100 (1992).
- [13] Feigenbaum, M.J., Quantitative universality for a class of nonlinear transformations, *J. Stat. Phys.* 19, 25-52 (1978).

- [14] Gonsalves, D.H., Neilson, R.D., Barr, A.D.S., A study of the response of a discontinuously nonlinear rotor system, *Nonlinear Dynamics* 7, 451-470 (1995).
- [15] Greenspan, B. & Holmes, P., Repeated resonance and homoclinic bifurcation in a periodically forced family of oscillators, *SIAM. J. Math. Anal.* 15(1), 69-97 (1984).
- [16] Guckenheimer, J. & Holmes, P., *Nonlinear Oscillations, Dynamical Systems and Bifurcations of Vector Fields* (Springer, New York, 1983).
- [17] van der Heijden, G.H.M., Mode-locking in nonlinear rotordynamics, *J. Nonlinear Sci.* 5, 257-283 (1995).
- [18] Hirschberg, P., Kirk, V. & Knobloch, E., Equivariant bifurcation analysis of localized patterns in excitable media, *Phys. Lett.* A172, 141-147 (1992).
- [19] Hirschberg, P. & Laing, C., Successive homoclinic tangencies to a limit cycle, *Physica* 89D, 1-14 (1995).
- [20] Iooss, G., A codimension 2 bifurcation for reversible vector fields, *Fields Institute Communications* 4, 201-217 (1995).
- [21] Kirk, V., Merging of resonance tongues, *Physica* 66D, 267-281 (1993).
- [22] Kirk, V., Breaking of symmetry in the saddle-node Hopf bifurcation, *Phys. Lett.* A154, 243-248 (1991).
- [23] MacKay, R.S., Tresser, C., Transition to topological chaos for circle maps, *Physica* 19D, 206-237 (1986).
- [24] Wiggins, S., *Global Bifurcations and Chaos* (Springer, New York, 1988).